INSTITUT DE FRANCE
Académie des sciences

Comptes Rendus

Mécanique

Yosra Kriaa, Amine Ammar and Bassem Zouari

Data-driven model based on the simulation of cracking process in brittle material using the phase-field method in application

Volume 348, issue 8-9 (2020), p. 729-744

Published online: 18 November 2020
Issue date: 14 December 2020

https://doi.org/10.5802/crmeca.52

Les Comptes Rendus. Mécanique *sont membres du Centre Mersenne pour l'édition scientifique ouverte*
www.centre-mersenne.org
e-ISSN : 1873-7234

Comptes Rendus
Mécanique
2020, 348, nº 8-9, p. 729-744
https://doi.org/10.5802/crmeca.52

Short paper / *Note*

Data-driven model based on the simulation of cracking process in brittle material using the phase-field method in application

Yosra Kriaa[*, a], **Amine Ammar**[b] **and Bassem Zouari**[a]

[a] LA2MP Laboratory, University of Sfax, National Engineering School of Sfax, Tunisia

[b] Arts et Metiers Institute of Technology, LAMPA, HESAM Université, F-49035 Angers, France

E-mails: yosra.2k@gmail.com (Y. Kriaa), amine.ammar@ensam.eu (A. Ammar), bzouari@yahoo.com (B. Zouari)

Abstract. Numerical simulations and parametric studies of notched rectangular specimens subjected to dynamic tensile loads were performed. The simulations were based on two-dimensional finite element analysis to predict the brittle fracture path using the phase-field approach. The parametric studies investigated the influence of geometric parameters and the loading speed on crack path propagation. An empirical model based on the sparse proper generalized decomposition learning technique was created to predict the crack path. This model provides a quick prediction of the global behavior of the crack path circumventing the CPU cost of the full finite element method simulation.

Keywords. Dynamic fracture propagation, Finite element, Brittle fracture, Phase-field approach, s-PGD technique.
Manuscript received 31st March 2020, revised and accepted 5th October 2020.

1. Introduction

Fracture is the primary cause of catastrophic structural failure. As no analytical solutions for crack propagation exist, except in a few special cases, accurate numerical modeling of the fracture is essential. In general, the numerical modeling of fracture can be performed using three classes of methods: (1) discrete modeling (cohesive zone modeling, extended finite element methods, and element deletion methods), (2) continuum damage description, and (3) phase-field methods.

Cohesive zone modeling requires either prior knowledge of the crack path (see Bhattacharjee *et al.* [1], Bhattacharjee [2], Barlingay [3]) or the insertion of a cohesive zone between all edges of the element as in Xu and Needleman [4], which increases the computational cost. Moreover, as the crack can propagate only along the finite element boundaries, different shapes of triangular elements can lead to different crack trajectories for the same boundary conditions as seen in Xu and Needleman [4]. The extended finite element method requires that the actual and predicted

* Corresponding author.

trajectories are verified at each step (see Moes and Belytschko [5]). In addition, since discontinuities have been injected based on a failure criterion, the use of level sets tends to favor the propagation of a single crack, which limits its use in cases of crack branching (Song *et al.* [6]). The element deletion method cannot predict the crack branching in the simulations performed by Song *et al.* [6]. In continuous damage models, a change in the character of governing partial differential equations occurs locally above a certain level of accumulated damage or plastic strains (Borst [7]). Thus, many existing methods are poorly suited for modeling the dynamic behavior of cracks.

Phase-field models can capture the complex behavior of cracks without any ad hoc criteria for crack evolution (Borden [8]) and are therefore effective in capturing the interactions between dynamically propagating cracks. In these approaches, the fracture surface is generated by a phase field (Borden *et al.* [9]). A continuous scalar-valued phase field α is introduced into the domain to indicate whether the material is in the damaged phase ($\alpha = 1$) or in the undamaged phase ($\alpha = 0$). The phase field is allowed to take intermediate values ($0 \leq \alpha \leq 1$) denoting a smearing of the crack over a small region characterized by a length-scale parameter η. It determines the stiffness of the material, that is, it reduces the strength of the material in areas where $\alpha > 0$. An equation for the evolution of this phase field is derived using Euler–Lagrange equations for a Lagrangian approximation to the fracture problem, which depends on the history of the strain energy of the domain and couples the equations for the evolution of the moment and the phase field. Besides, the equilibrium at a given moment is determined by solving this system of coupled equations. The phase-field method overcomes the many complexities of discrete fracture patterns. It does not require the numerical tracking of discontinuities or remeshing of the domain as the crack propagates. This allows the efficient modeling of crack branching (with a reduced computational time). This approach can also efficiently model fracture in three-dimensional problems (Borden *et al.* [9] and Wheeler *et al.* [10]) and can represent complex fracture surfaces simply by the phase-field variable.

The present research work follows that of Bourdin *et al.* [11], which implements the variational formulation for the growth of quasi-static cracks proposed by Francfort and Marigo [12]. The method uses a functional with two fields, the first of which is displacement and the second is a scalar phase field. Bourdin *et al.* [13] modify this formulation to model dynamic crack propagation. Miehe *et al.* [14] proposes a thermodynamically coherent phase-field formulation in which the fracture induced by the release of energy occurs only in tension. Other modifications include the introduction of a local history field that directs the evolution of the crack trajectory, making the formulation more robust; see Miehe *et al.* [15]. However, this formulation has a high computational cost since the balance of momentum equations becomes non-linear due to the split. This formulation has also limitations for modeling crack propagation problems under combined loading (Jeong *et al.* [16]). To overcome these problems, Ambati *et al.* [17] proposed a new formulation, which is a hybrid formulation. Borden [8] extends the phase-field formulation to ductile fracture and derives an approximation of the higher-order phase field for better accuracy. Recent notable extensions and improvements to the phase-field method include fracture modeling in rubbery polymers (Miehe and Schanzel [18]), thermo-elastic–plastic solids (Miehe *et al.* [19]) at large deformations, crack evolution in piezoelectric ceramics (Wilson *et al.* [20]), and pressure fractures (Wheeler *et al.* [10]).

In the remainder of this paper, we present a developed simulation from the phase-field model. Although this simulation is robust and gives precisely the complete crack path, it requires a refined mesh and has a rather high computational cost. However, the requirement is sometimes simpler. In fact, it is useful in some prediction cases to classify the cracks into two or three types of topologies and to determine the topology type resulting from the simulation according to the model parameters. Such an approach must then be based on learning techniques and must produce a meta-model based on data (data-driven).

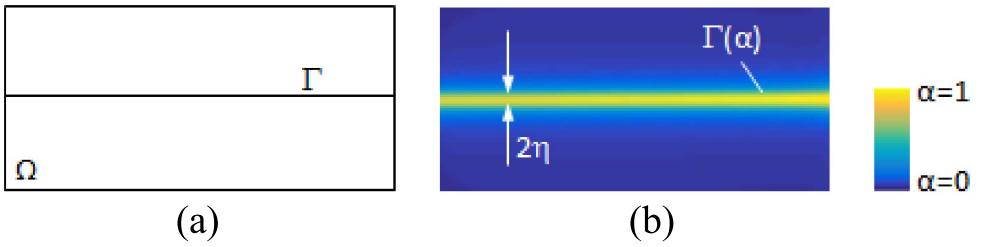

Figure 1. Body with an internal crack: (a) sharp crack; (b) diffusive crack.

In recent years, there has been growing interest in the integration of data-driven techniques in the mechanics field. In fact, in many scientific fields such as economy, sociology, and so on, big data are almost classical. However, in the field of computational mechanics, they have arrived significantly late. It should be noted that in this field, since the amount of data utilized is not very large, data-driven techniques rather than big-data techniques are applied more often. Among the first to integrate data-driven technologies into the field of computational mechanics are Kirchdoerfer and Ortiz [21, 22] and Brunton *et al.* [23–25]. More recently, the question of compliance with general laws such as those of thermodynamics has also been raised, which is a distinct feature of data-driven mechanics (Gonzalez *et al.* [26]). Other applications include the identification of biological systems (Mangan *et al.* [27]), financial trading (Mann and Kutz [28]), and so on.

In what follows, we use a method based on the concept of separate representations to overcome the curse of dimensionality. This separate representation has already been used by previous authors to construct a priori reduced-order modeling techniques called proper generalized decomposition (PGD) (Chinesta *et al.* [29–35]). Ibáñez *et al.* [36] have proposed a sparse proper generalized decomposition (s-PGD) approach to the problem and have shown the performance of this method in ten dimensions. This technique, which is based on the construction of a response surface in a parametric domain, whose dimension is relative to the number of parameters, is adopted in this research work. For the sum of tensor products, this method uses functions in spaces of dimension 1 relative to each parameter. The functions are estimated by a residual minimization procedure on training points in the parametric space.

We then show the ability of this meta-model to generate the topological prediction results on the test cases presented in Section 3.

2. Brittle fracture phase-field modeling

Consider a linear elastic body Ω. Let $\partial\Omega$ be the external boundary and Γ be the internal discontinuity or crack in the domain. Figure 1a shows a body Ω with discrete discontinuity Γ. Figure 1b shows the corresponding phase-field approximation, where the parameter η controls the width of the transition zone. The phase field α is a scalar field defined over the entire domain Ω such that $\alpha = 1$ denotes the fractured phase and $\alpha = 0$ denotes the unfractured phase.

According to Griffith's theory of brittle fracture, the energy required to create a unit surface area of fracture surface is equal to the critical fracture energy density G_c, which is also known as the fracture energy. The total potential energy E_{tot}, which is the sum of the elastic energy and the fracture energy, is given by Francfort and Marigo [12] as follows:

$$E_{\text{tot}} = \int_{\Omega} \psi_0(\boldsymbol{\varepsilon})\,\mathrm{d}\Omega + \int_{\Gamma} G_c\,\mathrm{d}\Gamma, \tag{1}$$

where Ψ_0, the elastic energy density, is a function of the strain field ε.

The kinetic energy of the body Ω is given as

$$\Psi_{\text{kin}}(\dot{\mathbf{u}}) = \frac{1}{2}\int_{\Omega} \rho\dot{\mathbf{u}}\cdot\dot{\mathbf{u}}\,\mathrm{d}\Omega. \tag{2}$$

The regularized form of the potential energy was proposed by Francfort and Marigo [12] and Bourdin *et al.* [37] by introducing the phase-field variable α.

The entire process of crack initiation and propagation is governed by a minimization problem of the regularized energy functional. It is parameterized by η and defined by the following equation:

$$E_{\text{tot}} = \int_{\Omega}\left[\frac{1}{2}\rho\dot{\mathbf{u}}\cdot\dot{\mathbf{u}} + ((1-\alpha)^2 + k(\eta))\psi_0(\boldsymbol{\varepsilon}(\mathbf{u}))\right]\mathrm{d}\Omega + \int_{\Omega} G_c\left[\frac{\alpha^2}{4\eta} + \eta\nabla\alpha\cdot\nabla\alpha\right]\mathrm{d}\Omega, \tag{3}$$

where u is the displacement field and $k(\eta) \ll 1$ is a parameter that prevents numerical singularity in the case of partly or fully broken systems. The length parameter η controls the width of the crack's smooth approximation.

To model the loss of stiffness in a fractured domain, the elastic potential energy Ψ_0 is split into two parts, Ψ_0^+ and Ψ_0^-, representing the elastic energy from tensile and compressive principal strains, respectively. To take into account the stiffness degradation under tensile stresses, Miehe *et al.* [38] defined Ψ_0 as follows:

$$\psi_0(\boldsymbol{\varepsilon},\alpha) = (1-\alpha)^2\psi_0^+(\boldsymbol{\varepsilon}) + \psi_0^-(\boldsymbol{\varepsilon}), \tag{4}$$

where

$$\psi_0^{\pm}(\varepsilon) = \tfrac{1}{2}\lambda\langle\mathrm{tr}(\varepsilon)\rangle_{\pm}^2 + \mu\,\mathrm{tr}(\varepsilon_{\pm}^2). \tag{5}$$

Herein, $\varepsilon_{\pm} = \sum_{I=1}^{3}\langle\varepsilon_I\rangle_{\pm}\mathbf{n}_I\otimes\mathbf{n}_I$ with $\{\varepsilon_I\}_{I=1}^3$ and $\{\mathbf{n}_I\}_{I=1}^3$ being the principal strains and principal strain directions, respectively, and $\langle a\rangle_{\pm} = (1/2)(a\pm|a|)$.

To take into account the loading and unloading histories, Miehe *et al.* [38] introduced the strain history functional

$$\mathrm{H}^+ = \max_{\tau\in[0,t]}\psi_0^+(\varepsilon(\mathbf{x},\tau)). \tag{6}$$

The anisotropic formulation is defined as

$$\begin{cases}\sigma(\mathbf{u},\alpha) = (1-\alpha)^2\dfrac{\partial\psi_0^+(\boldsymbol{\varepsilon})}{\partial\boldsymbol{\varepsilon}} + \dfrac{\partial\psi_0^-(\boldsymbol{\varepsilon})}{\partial\boldsymbol{\varepsilon}}\\ -4\eta^2\Delta\alpha + \alpha = \dfrac{4\eta}{G_c}(1-\alpha)\mathrm{H}^+.\end{cases} \tag{7}$$

To reduce the computational cost and overcome the limitation of the anisotropic formulation when the samples are subjected to combined tension and shear loading (Jeong *et al.* [16]), Ambati *et al.* [17] proposed the use of a hybrid formulation as follows:

$$\begin{cases}\sigma(\mathbf{u},\alpha) = (1-\alpha)^2\dfrac{\partial\psi_0(\boldsymbol{\varepsilon})}{\partial\boldsymbol{\varepsilon}}\\ -4\eta^2\Delta\alpha + \alpha = \dfrac{4\eta}{G_c}(1-\alpha)\mathrm{H}^+\\ \forall\mathbf{x}\colon \psi_0^+ < \psi_0^- \rightarrow \alpha = 0.\end{cases} \tag{8}$$

As in the anisotropic formulation, the crack evolution is driven only by the strain energy tensile part; it is therefore blocked under compression. Yet, contrary to the anisotropic formulation case, stiffness degradation occurs in all the directions of the material in the hybrid case.

Consequently, the completely broken part of the material cannot bear the load in any direction. The last constraint in (8) is adopted to prevent crack face interpenetration under compression (Ambati *et al.* [17]) resulting from complete stiffness degradation. Hence, the hybrid formulation is proposed in the present research work.

We used the staggered scheme, where the displacement and damage fields are updated alternatively. This scheme is chosen to ensure the robustness of the numerical solutions. Therefore, the Newmark algorithm to solve the displacement field problem u is adopted and then the damage field problem is solved as a linear system.

Thus, the dynamic problem consists in estimating the displacement and damage fields verifying the following equations, respectively:

$$\int_\Omega \rho\,\ddot{u}\cdot\delta u\,\mathrm{d}\Omega + \int_\Omega \left[((1-\alpha)^2 + k(\eta))\frac{\partial \psi_0}{\partial \varepsilon}(\varepsilon(u))\right] : \delta\varepsilon\,\mathrm{d}\Omega = 0 \tag{9}$$

$$2\int_\Omega \alpha\beta{\psi_0}^+(\varepsilon(u))\,\mathrm{d}\Omega + \int_\Omega \frac{G_c}{2\eta}\alpha\delta\alpha\,\mathrm{d}\Omega + \int_\Omega 2G_c\eta\nabla\alpha\nabla\delta\alpha\,\mathrm{d}\Omega = 2\int_\Omega \delta\alpha{\psi_0}^+(\varepsilon(u))\,\mathrm{d}\Omega. \tag{10}$$

The Newmark algorithm below is used to solve (9):

1. Data: mesh, (E, υ, ρ), initial conditions: $\{U_0\}$ and $\{\dot{U}_0\}$
2. Assembly of the stiffness and the mass matrix: $[K]$ and $[M]$
3. Initialization: calculation of $\{\ddot{U}_0\}$ **with:** $[M]\{\ddot{U}_0\} = \{F_0\} - [K]\{U_0\}$
4. Matrix construction and factorization: $[S] = [M] + \beta\Delta t^2[K]$
5. For $n = 0$ **to** $N-1$ **do**
6. Prediction: $\begin{cases} \{U_{n+1}^{\mathrm{pred}}\} = \{U_n\} + \Delta t\{\dot{U}_n\} + \frac{1}{2}\Delta t^2(1-2\beta)\{\ddot{U}_n\} \\ \{\dot{U}_{n+1}^{\mathrm{pred}}\} = \{\dot{U}_n\} + \Delta t(1-\gamma)\{\ddot{U}_n\} \end{cases}$
7. Calculation of the acceleration by: $[S]\{\ddot{U}_{n+1}\} = \{F_{n+1}\} - [K_d]\{U_{n+1}^{\mathrm{pred}}\}$
8. Correction and update: $\begin{cases} \{U_{n+1}\} = \{U_{n+1}^{\mathrm{pred}}\} + \Delta t^2\beta\{\ddot{U}_{n+1}\} \\ \{\dot{U}_{n+1}\} = \{\dot{U}_{n+1}^{\mathrm{pred}}\} + \Delta t\gamma\{\ddot{U}_{n+1}\} \end{cases}$
9. End for

After discretization, Equation (10) becomes

$$2G_c\eta R\begin{pmatrix}\alpha_1\\ \vdots\\ \alpha_{N_s}\end{pmatrix} + \left(2\psi_0(\varepsilon(u)) + \frac{G_c}{2\eta}\right)M\begin{pmatrix}\alpha_1\\ \vdots\\ \alpha_{N_s}\end{pmatrix} = 2\psi_0(\varepsilon(u))N, \tag{11}$$

where

$$R = \sum_{k=1}^{N_t} r_k;\quad r_k = \begin{pmatrix} \int_{T_k}\nabla\varphi_i^2\,\mathrm{d}T_k & \int_{T_k}\nabla\varphi_i\nabla\varphi_j\,\mathrm{d}T_k & \int_{T_k}\nabla\varphi_i\nabla\varphi_l\,\mathrm{d}T_k \\ \int_{T_k}\nabla\varphi_j\nabla\varphi_i\,\mathrm{d}T_k & \int_{T_k}\nabla\varphi_j^2\,\mathrm{d}T_k & \int_{T_k}\nabla\varphi_j\nabla\varphi_l\,\mathrm{d}T_k \\ \int_{T_k}\nabla\varphi_l\nabla\varphi_i\,\mathrm{d}T_k & \int_{T_k}\nabla\varphi_l\nabla\varphi_j\,\mathrm{d}T_k & \int_{T_k}\nabla\varphi_l^2\,\mathrm{d}T_k \end{pmatrix},$$

$$M = \sum_{k=1}^{N_t} m_k;\quad m_k = \begin{pmatrix} \int_{T_k}\varphi_i^2\,\mathrm{d}T_k & \int_{T_k}\varphi_i\varphi_j\,\mathrm{d}T_k & \int_{T_k}\varphi_i\varphi_l\,\mathrm{d}T_k \\ \int_{T_k}\varphi_j\varphi_i\,\mathrm{d}T_k & \int_{T_k}\varphi_j^2\,\mathrm{d}T_k & \int_{T_k}\varphi_j\varphi_l\,\mathrm{d}T_k \\ \int_{T_k}\varphi_l\varphi_i\,\mathrm{d}T_k & \int_{T_k}\varphi_l\varphi_j\,\mathrm{d}T_k & \int_{T_k}\varphi_l^2\,\mathrm{d}T_k \end{pmatrix},\quad \text{and}$$

$$N = \sum_{k=1}^{N_t} n_k;\quad n_k = \begin{pmatrix} \int_{T_k}\varphi_i\,\mathrm{d}T_k \\ \int_{T_k}\varphi_j\,\mathrm{d}T_k \\ \int_{T_k}\varphi_l\,\mathrm{d}T_k \end{pmatrix}. \tag{12}$$

Therefore, it is a linear problem like the quasi-static problem:

$$K_\alpha^+(U)\alpha = F_\alpha^+ \tag{13}$$

with

$$\begin{cases} K_\alpha^+(U) = 2G_c\eta R + \left(2\psi_0^+(\varepsilon(u)) + \dfrac{G_c}{2\eta}\right)M \\ F_\alpha^+ = 2\psi_0^+(\varepsilon(u))N. \end{cases} \tag{14}$$

3. The s-PGD technique

The s-PGD technique is applied in the proposed case in a three-dimensional space (we are using a three-dimensional parametric space). We denote by x_i, y_i, z_i the coordinates of training simulation parameters in the parametric space. The parameter f_i is a global observable that we can extract from the simulation (it could be for example a topology type of the crack path). The parameter $f(x, y, z)$ is then a function defined only on some P points used for training. The purpose of the s-PGD technique is to look for the best continuous function $u(x, y, z)$ such that the error defined in (15) is minimum:

$$\sum_{i=1}^{P}(u(x_i, y_i, z_i) - f_i)^2. \tag{15}$$

This technique detailed in Ibáñez *et al.* [36] allows writing the solution as an interpolation with separate one-dimensional functions:

$$u(x, y, z) = \sum_{j=1}^{M} F^j(x)G^j(y)H^j(z). \tag{16}$$

Many choices are possible for the basis on which the functions F^j, G^j, H^j are expressed. In the proposed case, the Chebyshev polynomials are adopted. Thus, if we denote by $L_k, k = 1 \dots K$ the first K Chebyshev polynomial functions, then the expressions of the functions F^j, G^j, H^j are given by

$$\begin{aligned} F^j &= \alpha_1^j L_1 + \cdots + \alpha_K^j L_K, \\ G^j &= \beta_1^j L_1 + \cdots + \beta_K^j L_K, \\ H^j &= \gamma_1^j L_1 + \cdots + \gamma_K^j L_K. \end{aligned} \tag{17}$$

Consequently, the s-PGD technique consists in finding the set of coefficients $\alpha_k^j, \beta_k^j, \gamma_k^j$ for each mode j.

4. The data-driven model

In this section, the performance of the s-PGD in predicting the type of fracture path, related to geometric specimen parameters and the load velocity, is compared to that of the phase-field direct numerical simulation.

Two specimen geometries subject to dynamic tensile tests were studied, namely the double-notched specimen and the pre-notched rectangular plate with a central hole.

4.1. *Tensile test of double-notched specimens*

In this subsection, we describe the test of double-notched rectangular specimens under tensile stress. We investigate the influence on the crack trajectory of the radius of two circular notches (v_1), the axial distance between them (v_2), and the loading speed (v_3). The geometry, boundary

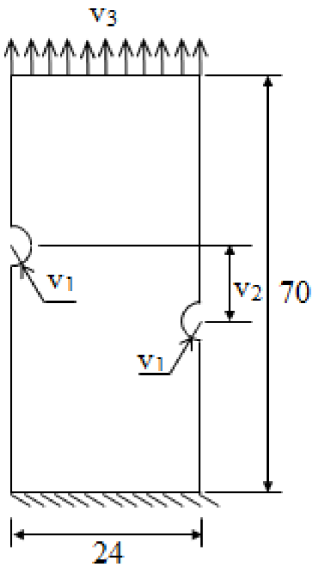

Figure 2. Tensile test: geometry and boundary conditions.

conditions, and loading are illustrated in Figure 2. The loading is given by applying normal displacements, at fixed velocity $v3$, on the upper border of the plate $u = v_3 \times t$, and the lower edge is assumed to be fixed. The other boundaries are free. The specimen is discretized by triangular plane stress elements and an effective element size of $h = 0.2$ mm in the fracture propagation zone. The material parameters are density $\rho = 7800\,\text{kg/m}^3$, Young's modulus $E = 210$ GPa, Poisson ratio $v = 0.3$, and critical fracture energy density $G_c = 0.05$ kN/mm. The selected length-scale parameter is $\eta = 2h = 0.4$ mm. The time step is set as $\Delta t = 10^{-4}$ ms.

Two types of crack paths, namely a crack propagation from notch to notch and a propagation from notch to edge, can be distinguished. Figure 3a shows an example of a crack propagating horizontally from the left notch and deviating to the vicinity of the right notch and at the same time another crack spreading from the right notch to the left notch. Figure 3b shows an example of a crack propagating horizontally from the left notch to the right edge and another crack spreading from the right notch to the left edge.

The crack pattern depends notably on the chosen three parameters. Table 1 lists the 15 sets of input parameters used for training, which are chosen by the lhsdesign Matlab function, and their associated results from direct numerical simulation.

At this stage, it is important to define the output. Indeed, if the crack propagates between the two circular notches, we fix the output at the value 1; if not, the output is fixed at 0. Once the training stage is performed, we choose seven other validation tests included in the same parametric space to which the training parameters belong. This set of parameters is presented in Table 2. The crack trajectory for all the training and validation tests is summarized in Supplementary Appendix 1.

The training is illustrated in Figure 4. The circle and cross symbols are used to express the output values 1 and 0, respectively, in the parametric space. As the s-PGD prediction technique does not generate a binary value, we decided to reduce the output values greater than 0.5 to 1, and those lower than 0.5 to 0. The dot and plus symbols are used to represent these two situations, respectively. Figure 4 reveals that the built function matches the expected output at least for the training points.

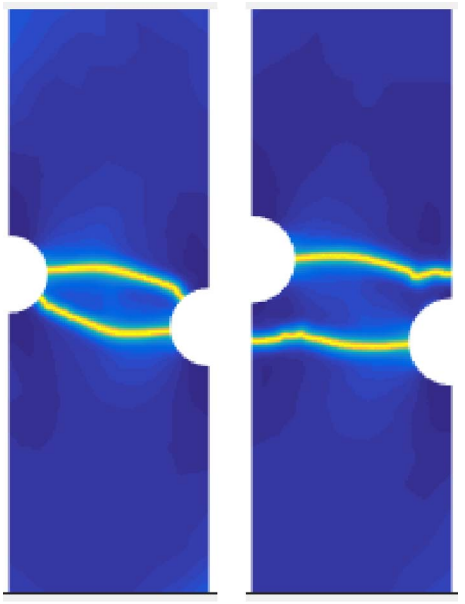

Figure 3. Crack paths on the plate with two circular notches: (a) crack propagates from the left notch to the right notch; (b) crack propagates horizontally from the left notch to the right edge.

Table 1. Results for 15 simulations with the phase-field method of double-notched rectangular specimens

Training simulation number	Radius of two circular notches (v_1)	Axial distance between two circular notches (v_2)	Load velocity (v_3)	Output of the phase-field model
1	6.9236	8.6796	5.346	1
2	4.6531	6.3371	6.7498	1
3	3.2944	3.2928	3.4169	1
4	4.4407	9.2565	2.2072	0
5	5.9643	7.7261	4.6815	1
6	6.215	3.9644	4.3667	1
7	4.9869	5.4881	8.5272	1
8	5.2058	9.9035	8.052	0
9	6.5795	6.8949	7.1293	1
10	3.7931	8.5664	1.6703	0
11	4.2143	4.6769	1.0518	1
12	3.0943	5.0221	6.065	1
13	3.9277	5.8309	3.0407	1
14	5.5674	3.5549	9.3107	1
15	5.6834	7.4405	9.4602	1

Figure 5 shows the points used for validation (controlled prediction) in the parametric space. It proves that the data-driven model is able to correctly predict the crack path behavior in points

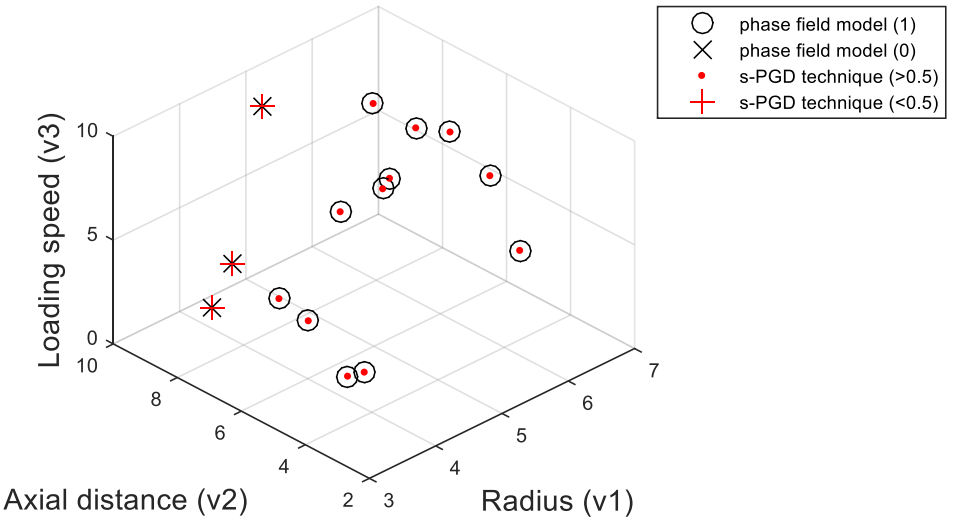

Figure 4. Results for 15 tests with the s-PGD technique.

Table 2. Results for seven simulations used for validation of double-notched rectangular specimens

Validation simulation number	Radius of two circular notches (v_1)	Axial distance between two circular notches (v_2)	Load velocity (v_3)	Results of the phase-field model
1	4.237	4.1573	5.6813	1
2	6.6541	9.4527	1.8516	1
3	3.6541	9.4527	3.8516	0
4	3.1397	7.4361	9.2498	0
5	5.3332	6.0753	3.4177	1
6	6.0935	5.7153	7.0696	1
7	3.2	8.5	8	0

that are not used for training (the circle symbol matches the dot symbol and the symbols "×" and "+" match as well).

Finally, to make a non-controlled prediction, Figure 6 shows the expected output (between 0 and 1) for 2000 points randomly distributed on the parametric space. Such a figure could be very useful for predicting the crack path topology quickly for a given set of parameters. It is also useful for localizing the region in the parametric space where there is uncertainty about the crack path topology (output approximately 0.5).

4.2. *Tensile test of pre-notched specimens with a central hole*

In this subsection, we describe the test of notched rectangular specimens under tensile stress. We investigate the influence of the hole radius (v_1), the distance between the pre-notch and the hole (v_2), and the loading speed (v_3) on the crack trajectory. The geometry, boundary conditions, and loading are illustrated in Figure 7. In fact, a normal displacement is applied on the upper border of the plate $u = v_3 \times t$, the lower edge is assumed to be fixed, and the other boundaries are free. The specimen is discretized with triangular plane stress elements and an effective size of $h = 0.2$ mm

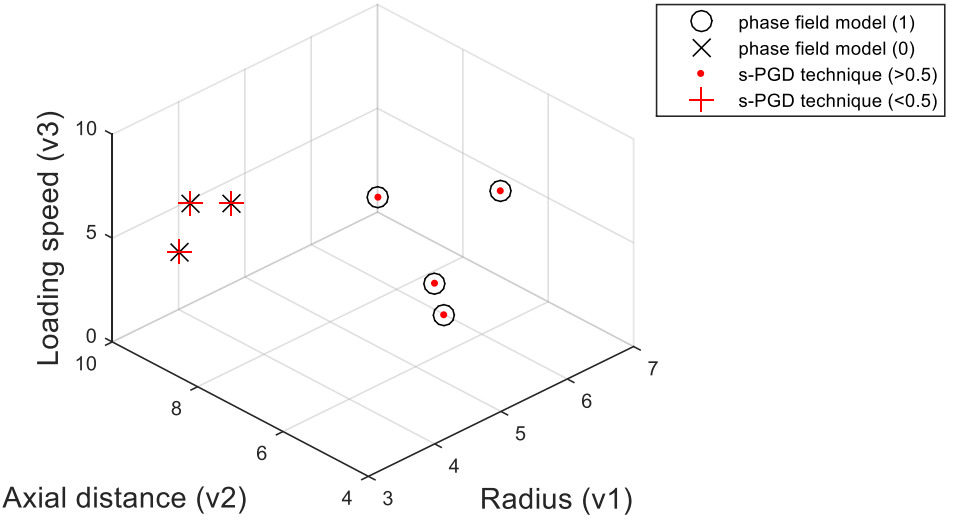

Figure 5. Results for seven tests of validation with the s-PGD technique.

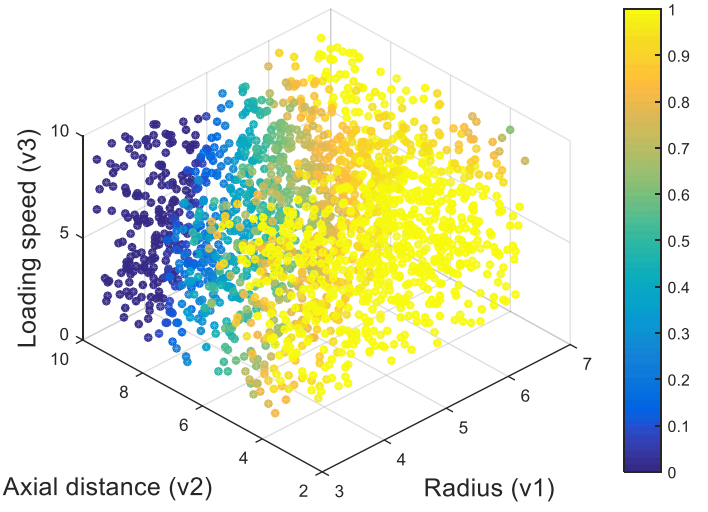

Figure 6. Results for the s-PGD technique.

in the fracture propagation zone. The material parameters are $\rho = 7800$ kg/m^3, $E = 210$ GPa, $\upsilon = 0.3$, and $G_c = 0.05$ kN/mm. The selected length-scale parameter is $\eta = 2h = 0.4$ mm. The time step is set as $\Delta t = 10^{-4}$ ms.

It is worth noting that two types of crack paths are distinguishable in this case. Regarding the first, it is a propagation from the pre-crack toward the hole and then from the hole to the right edge (Figure 8a). As regards the second, it is a horizontal propagation from the pre-crack to the right edge without deviation to the hole (Figure 8b).

The crack pattern depends notably on the set of parameters. Table 3 shows the training simulation parameters and their associated results obtained using the phase-field method.

At this juncture, it is important to define the output. If the crack runs through the hole, we fix the output at the value 1; if not, the output is fixed at 0. Once the training stage is performed,

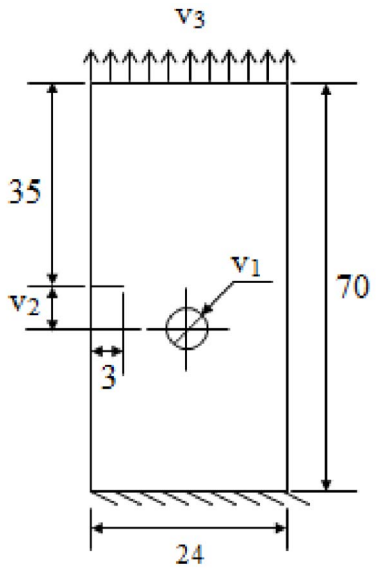

Figure 7. Tensile test: geometry and boundary conditions.

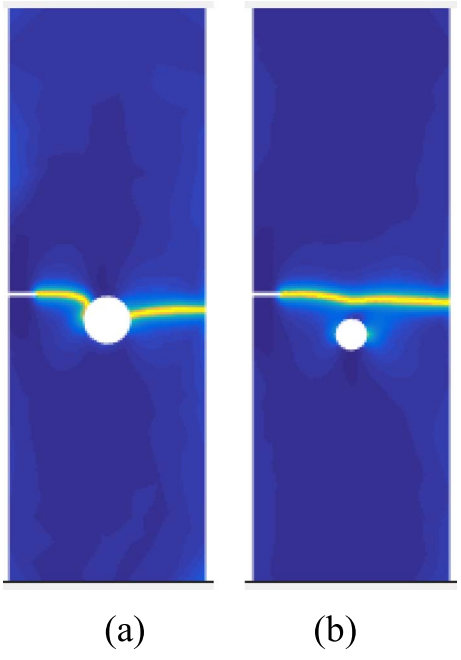

Figure 8. Crack paths on the plate with notch and hole: (a) crack deviates through the hole; (b) crack propagates horizontally.

we choose five other validation tests included in the same parametric space to which the training parameters belong (Table 4). The crack trajectory for all the training and validation tests is summarized in Supplementary Appendix 2.

Table 3. Results for 15 simulations with the phase-field method for pre-notched specimens with a central hole

Training simulation number	Radius of the hole ($v1$)	Distance between the pre-crack and the hole ($v2$)	Load velocity ($v3$)	Output of the phase-field model
1	2.886	2.8921	1.8595	1
2	1.9156	4.6428	1.1035	0
3	1.617	6.3816	6.1651	0
4	1.728	6.5986	7.8274	0
5	3.4916	3.4409	3.421	1
6	2.8142	7.062	2.3032	0
7	1.891	5.1391	8.3116	0
8	3.2086	8.2394	9.4267	0
9	2.9976	8.378	5.0905	0
10	2.3136	4.6043	4.1977	1
11	3.2976	9.4882	5.3587	0
12	2.5874	5.6011	2.908	1
13	2.1362	9.2054	8.9911	0
14	2.2428	7.685	6.8023	0
15	2.5176	3.9974	7.579	1

Table 4. Results for five simulations used for validation of pre-notched specimens with a central hole

Validation simulation number	Radius of the hole ($v1$)	Distance between the pre-crack and the hole ($v2$)	Load velocity ($v3$)	Output of the phase-field model
1	2.533	6.5224	2.8075	0
2	1.7828	8.1331	9.2141	0
3	2.0191	3.3723	7.652	1
4	3.4041	4.4432	2.3563	1
5	2.7162	9.1286	4.6705	0

Figure 9 shows the results of the 15 training tests. The circle and cross symbols are used to express the output values 1 and 0, respectively, in the parameter space. Since the s-PGD prediction technique does not generate a binary value, we decided to reduce the output values greater than 0.5 to 1 and those lower than 0.5 to 0. The dot and plus symbols are used to represent these two situations, respectively. Figure 9 shows that the constructed function corresponds to the expected output at least for the training points with the exception of one test. As illustrated in Figure 10, for this set of parameters, the crack propagates horizontally from the notch and deviates to the vicinity of the hole on the right side and then propagates from the hole to the right edge. As a result, this test creates a singularity and the two methods do not give the same results.

Figure 11 shows the points in the parametric space used for validation (controlled prediction). This figure reveals that the data-driven model is able to correctly predict the behavior of the crack path in points that are not used for training (the circle symbol matches the dot symbol and the symbols "×" and "+" match likewise).

Finally, to make a non-controlled prediction, Figure 12 shows the expected output (between 0 and 1) for 2000 points randomly distributed on the parametric space. This figure could be very

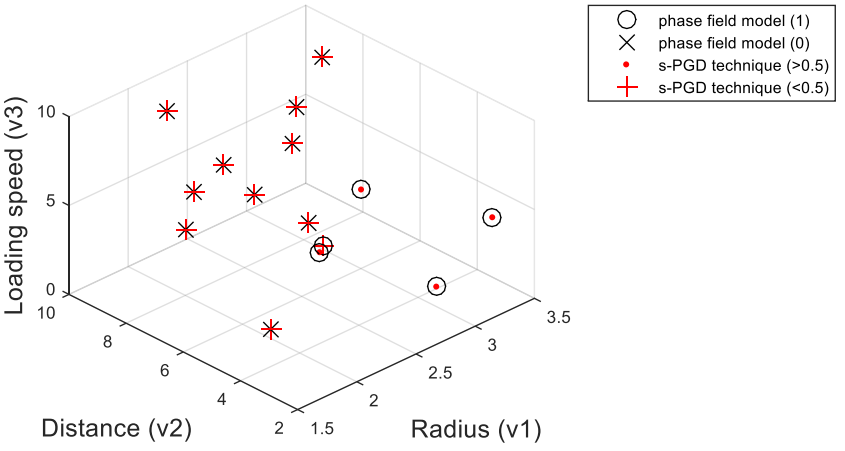

Figure 9. Results for 15 tests with the s-PGD technique.

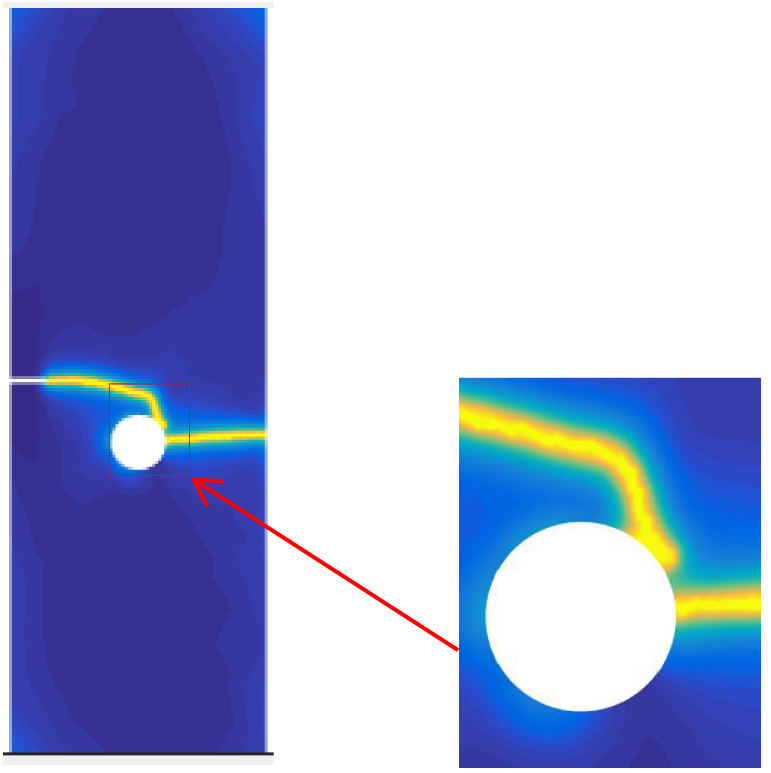

Figure 10. Crack paths on the plate with notch and hole: critical case.

useful when it comes to locating the parameters to obtain the type of topology. It is also useful for locating the region of the parametric space where we have some uncertainty about the crack path topology (output approximately 0.5).

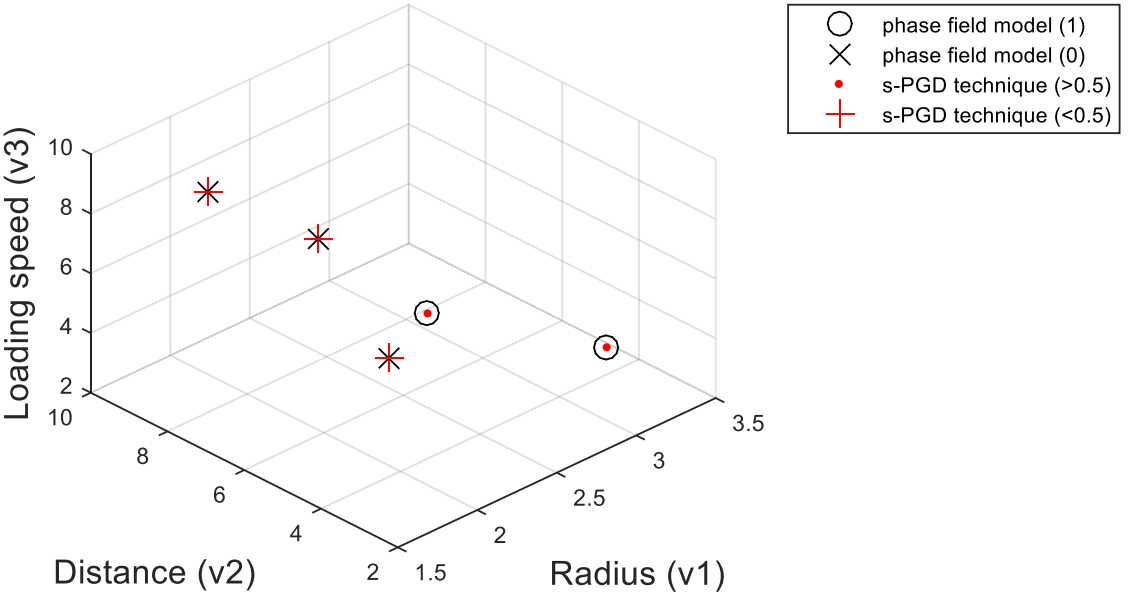

Figure 11. Results for five tests of validation with the s-PGD technique.

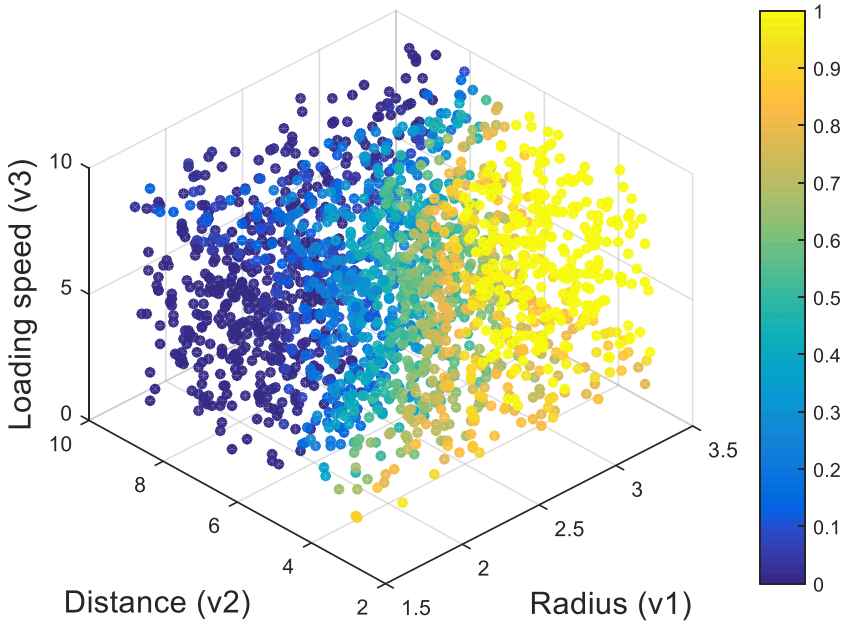

Figure 12. Results for the s-PGD technique.

5. Conclusion

The phase-field modeling of brittle fracture is a promising computational tool for tackling fracture problems with complex topologies for crack paths. The direct numerical simulation method is often expensive in terms of CPU cost. This research work presents an application using the s-PGD technique for the construction of a meta-model based on data. This study is performed on

only three parameters (two geometrical parameters and load velocity). At this level, the results are satisfactory. A possible extension could include the variability effects of material parameters or phase-field parameters. However, when the parametric space dimension increases, the number of training simulations must be sufficiently significant. Otherwise, some constraints must be applied on the s-PGD technique to avoid high-order solutions. It is noteworthy that this point constitutes a work in progress.

Supplementary data

Supporting information for this article is available on the journal's website under https://doi.org/10.5802/crmeca.52 or from the author.

References

[1] T. Bhattacharjee, M. Barlingay, H. Tasneem, E. Roan, K. Vemaganti, "Cohesive zone modeling of mode I tearing in thin soft materials", *J. Mech. Behav. Biomed. Mater.* **28** (2013), p. 37-46.
[2] T. Bhattacharjee, "Cohesive zone modeling of tearing in soft materials", Master's thesis, University of Cincinnati (2011).
[3] M. Barlingay, "Modeling and simulation of tissue tearing and failure for surgical applications", Master's thesis, University of Cincinnati (2012).
[4] X.-P. Xu, A. Needleman, "Numerical simulations of fast crack growth in brittle solids", *J. Mech. Phys. Solids* **42** (1994), no. 9, p. 1397-1434.
[5] N. Moes, T. Belytschko, "Extended finite element method for cohesive crack growth", *Eng. Fract. Mech.* **69** (2002), no. 7, p. 813-833.
[6] J.-H. Song, H. Wang, T. Belytschko, "A comparative study on finite element methods for dynamic fracture", *Comput. Mech.* **42** (2008), no. 2, p. 239-250.
[7] R. Borst, "Damage, material instabilities, and failure", in *Encyclopedia of Computational Mechanics, Vol. II*, Wiley, 2004, p. 335-375.
[8] M. J. Borden, Isogeometric analysis of phase-field models for dynamic brittle and ductile fracture, Ph.D. thesis, The University of Texas at Austin (2012).
[9] M. J. Borden, C. V. Verhoosel, M. A. Scott, T. J. Hughes, C. M. Landis, "A phase-field description of dynamic brittle fracture", *Comput. Methods Appl. Mech. Eng.* **217–220** (2012), p. 77-95.
[10] M. Wheeler, T. Wick, W. Wollner, "An augmented-lagrangian method for the phase-field approach for pressurized fractures", *Comput. Methods Appl. Mech. Eng.* **271** (2014), p. 69-85.
[11] B. Bourdin, G. A. Francfort, J.-J. Marigo, "Numerical experiments in revisited brittle fracture", *J. Mech. Phys. Solids* **48** (2000), no. 4, p. 797-826.
[12] G. A. Francfort, J.-J. Marigo, "Revisiting brittle fracture as an energy minimization problem", *J. Mech. Phys. Solids* **46** (1998), no. 8, p. 1319-1342.
[13] B. Bourdin, C. J. Larsen, C. L. Richardson, "A time-discrete model for dynamic fracture based on crack regularization", *Int. J. Fract.* **168** (2011), no. 2, p. 133-143.
[14] C. Miehe, F. Welschinger, M. Hofacker, "Thermodynamically consistent phase-field models of fracture: Variational principles and multi-field implementations", *Int. J. Numer. Methods Eng.* **83** (2010), no. 10, p. 1273-1311.
[15] C. Miehe, M. Hofacker, F. Welschinger, "A phase field model for rate-independent crack propagation: Robust algorithmic implementation based on operator splits", *Comput. Methods Appl. Mech. Eng.* **199** (2010), no. 45, p. 2765-2778.
[16] H. Jeong, S. Signetti, T. Seok Han, S. Ryu, "Phase field modeling of crack propagation under combined shear and tensile loading with hybrid formulation", *Comput. Mater. Sci.* **155** (2018), p. 483-492.
[17] M. Ambati, T. Gerasimov, L. De Lorenzis, *A Review on Phase-Field Models of Brittle Fracture and A New Fast Hybrid Formulation*, Springer-Verlag, Berlin, Heidelberg, 2014.
[18] C. Miehe, L.-M. Schanzel, "Phase field modeling of fracture in rubbery polymers. Part I: Finite elasticity coupled with brittle failure", *J. Mech. Phys. Solids* **65** (2014), p. 93-113.
[19] C. Miehe, M. Hofacker, L.-M. Schaenzel, F. Aldakheel, "Phase field modeling of fracture in multi-physics problems. Part II: coupled brittle-to-ductile failure criteria and crack propagation in thermo-elastic plastic solids", *Comput. Methods Appl. Mech. Eng.* **294** (2015), p. 486-522.
[20] Z. A. Wilson, M. J. Borden, C. M. Landis, "A phase-field model for fracture in piezoelectric ceramics", *Int. J. Fract.* **183** (2013), no. 2, p. 135-153.

[21] T. Kirchdoerfer, M. Ortiz, "Data-driven computational mechanics", *Comput. Methods Appl. Mech. Eng.* **304** (2016), p. 81-101.
[22] T. Kirchdoerfer, M. Ortiz, "Data driven computing with noisy material data sets", *Comput. Methods Appl. Mech. Eng.* **326** (2017), p. 622-641.
[23] S. L. Brunton, J. L. Proctor, J. N. Kutz, "Discovering governing equations from data by sparse identifcation of nonlinear dynamical systems", *Proc. Natl Acad. Sci. USA* **113** (2016), no. 15, p. 3932-3937.
[24] S. L. Brunton, J. L. Proctor, J. N. Kutz, "Sparse identifcation of nonlinear dynamics with control", *IFAC* **49** (2016), no. 18, p. 710-715.
[25] M. Quade, M. Abel, J. N. Kutz, S. L. Brunton, "Sparse identifcation of nonlinear dynamics for rapid model recovery", *Chaos* **28** (2018), no. 6, article no. 063116 (10 pages).
[26] D. Gonzalez, F. Chinesta, E. Cueto, "Termodynamically consistent data-driven computational mechanics", *Contin. Mech. Termodyn.* **31** (2019), p. 239-253.
[27] N. M. Mangan, S. L. Brunton, J. L. Proctor, J. N. Kutz, "Inferring biological networks by sparse identifcation of nonlinear dynamics", *IEEE Trans. Mol. Biol. Multi-Scale Commun.* **2** (2016), no. 1, p. 52-63.
[28] J. Mann, J. N. Kutz, "Dynamic mode decomposition for fnancial trading strategies", *Quant. Finance* **16** (2016), no. 11, p. 1643-1655.
[29] F. Chinesta, A. Ammar, E. Cueto, "Recent advances and new challenges in the use of the proper generalized decomposition for solving multidimensional models", *Arch. Comput. Methods Eng.: State-of-the-Art Reviews* **17** (2010), no. 4, p. 327-350.
[30] F. Chinesta, R. Keunings, A. Leygue, *The Proper Generalized Decomposition for Advanced Numerical Simulations*, Springer Briefs in Applied Sciences and Technology, Springer, Cham, 2014.
[31] F. Chinesta, P. Ladeveze, *Separated Representations and PGD-Based Model Reduction*, CISM International Centre for Mechanical Sciences, Courses and Lectures, vol. 554, Springer, Vienna, 2014.
[32] D. Gonzalez, A. Ammar, F. Chinesta, E. Cueto, "Recent advances on the use of separated representations", *Int. J. Numer. Methods Eng.* **81** (2010), no. 5, p. 637-659.
[33] A. Badas, D. Gonzalez, I. Alfaro, F. Chinesta, E. Cueto, "Local proper generalized decomposition", *Int. J. Numer. Methods Eng.* **112** (2017), no. 12, p. 1715-1732.
[34] E. Cueto, D. Gonzalez, I. Alfaro, *Proper Generalized Decompositions*, Springer Briefs in Applied Sciences and Technology, Springer, Cham, 2016.
[35] D. Gonzalez, A. Badas, I. Alfaro, F. Chinesta, E. Cueto, "Model order reduction for real-time data assimilation through extended Kalman flters", *Comput. Methods Appl. Mech. Eng.* **326** (2017), p. 679-693.
[36] R. Ibáñez, E. Abisset-Chavanne, A. Ammar, D. González, E. Cueto, A. Huerta, J. L. Duval, F. Chinesta, "A multidimensional data-driven sparse identification technique: The sparse proper generalized decomposition", *Hindawi Complexity* (2018), p. 1-11, doi:10.1155/2018/5608286.
[37] B. Bourdin, G. A. Francfort, J. J. Marigo, *The Variational Approach to Fracture*, Springer, Berlin, 2008.
[38] C. Miehe, M. Hofacker, F. Welschinger, "A phase field model for rate-independent crack propagation: Robust algorithmic implementation based on operator splits", *Comput. Methods Appl. Mech. Eng.* **199** (2010), no. 45–48, p. 2765-2778.